

The association between cerebrovascular reactivity and resting-state fMRI functional connectivity in healthy adults: The influence of basal carbon dioxide

Ali M. Golestani^a, Jonathan B. Kwinta^{a,b,1}, Stephen C. Strother^{a,b}, Yasha B. Khatamian^a, and J. Jean Chen^{a,b,*}

^aRotman Research Institute at Baycrest Centre, Canada

^bDepartment of Medical Biophysics, University of Toronto, Canada

Abstract

Although widely used in resting-state fMRI (fMRI) functional connectivity measurement (fcMRI), the BOLD signal is only an indirect measure of neuronal activity, and is inherently modulated by both neuronal activity and vascular physiology. For instance, cerebrovascular reactivity (CVR) varies widely across individuals irrespective of neuronal function, but the implications for fcMRI are currently unknown. This knowledge gap compromises our ability to correctly interpret fcMRI measurements. In this work, we investigate the relationship between CVR and resting fcMRI measurements in healthy young adults, in both the motor and the executive-control networks. We modulate CVR within each individual by subtly increasing and decreasing resting vascular tension through baseline end-tidal CO₂ (PETCO₂), and measure fcMRI during these hypercapnic, hypocapnic and normocapnic states. Furthermore, we assess the association between CVR and fcMRI within and across individuals. Within individuals, resting PETCO₂ is found to significantly influence both CVR and resting fcMRI values. In addition, we find resting fcMRI to be significantly and positively associated with CVR across the group in both networks. This relationship is potentially mediated by concomitant alterations in BOLD signal fluctuation amplitude. This work clearly demonstrates and quantifies a major vascular modulator of resting fcMRI, one that is also subject and regional dependent. We suggest that individualized correction for CVR effects in fcMRI measurements is essential for fcMRI studies of healthy brains, and can be even more important in studying diseased brains.

Keywords

Resting-state functional connectivity (fcMRI); Resting-state BOLD fMRI (rs-fMRI); Cerebrovascular reactivity (CVR); End-tidal CO₂ (PETCO₂); Vascular tension; Amplitude of low-frequency fluctuations (ALFF)

*Corresponding author at: Rotman Research Institute, Baycrest, 3560 Bathurst Street, Toronto, Ontario M6A 2E1, Canada., jchen@research.baycrest.org (J.J. Chen).

¹co-first author.

Disclosure/conflict of interest

The authors declare no conflict of interest.

Introduction

Functional magnetic resonance imaging (fMRI) in the resting state (rs-fMRI), particularly based on the blood oxygen level-dependent (BOLD) signal, has been extensively used to measure functional connectivity in the brain. This technique has been referred to as “rs-fcMRI” (Birn et al., 2014; Tak et al., 2015). This rs-fcMRI technique is widely used in neuroscience research, and has vast potential for studying patients and the elderly, for whom task performance in conventional fMRI may be difficult due to reduced cognitive and motor capacity. However, this tremendous potential is severely undermined by the current lack of a fundamental physiological understanding of the underlying rs-fMRI BOLD signal (Leopold and Maier, 2012). The BOLD signal is only an indirect measure of neuronal activity, and is inherently modulated by both neuronal activity and vascular physiology (Biswal and Kannurpatti, 2009; Biswal et al., 2007; Kannurpatti et al., 2008; Tong and Frederick, 2010). Currently, the respective contributions of these factors to resting-state BOLD are still unknown in the healthy brain. This leads to great challenges for data interpretation in clinical scenarios, whereby these contributions are often altered.

The literature suggests that BOLD-based fMRI signal is fundamentally modulated by local vascular physiology (Carusone et al., 2002; Kannurpatti et al., 2010; Liu et al., 2013). The coupling between neuronal metabolism and vascular activity is central to the ability of fMRI techniques such as BOLD to map neuronal activity. This relationship can be summarized by the BOLD biophysical model (Davis et al., 1998; Hoge et al., 1999),

$$\frac{\Delta \text{BOLD}}{\text{BOLD}_0} = M \left(1 - \left(\frac{\text{CMRO}_2}{\text{CMRO}_{2|0}} \right)^\beta \left(\frac{\text{CBF}}{\text{CBF}_0} \right)^{\alpha-\beta} \right) \quad (1)$$

where CMRO_2 is cerebral metabolic rate of oxygen, CBF is cerebral blood flow, α , β and M are constants which depend on physiological and acquisition parameters, and the subscript ‘0’ denotes baseline. Specifically,

$$M = A \cdot \text{TE} \cdot \text{CBF}_0^\alpha \cdot [\text{dHb}]_0^\alpha \quad (2)$$

where A is a constant, TE is the BOLD echo time, and [dHb] is the deoxyhemoglobin concentration. The above formulation allows us to appreciate the key role of the vascular term, CBF/CBF_0 , which depends on the degree of neurovascular coupling and cerebrovascular reactivity (CVR). In terms of Eq. (1), CVR is an important factor in determining the extent of CBF response to CMRO_2 changes (Maggio et al., 2014). One can also appreciate that CVR, which does not have direct neuronal effects, can substantially modulate the BOLD signal and thus introduce ambiguity into the measurement interpretations, particularly in the presence of vascular pathology. Such interactions have been reported previously for task-related BOLD response (Liu et al., 2013).

Often measured as the degree of vasodilatation in response to non-neural stimuli such as moderate changes in end-tidal pressure of carbon dioxide (PETCO_2), CVR has been widely

used to characterize diseases (Packard et al., 2003; Ziyeh et al., 2005), as it is linked to vascular reserve and autoregulatory capacity (Nur et al., 2009). CVR also covaries with the BOLD response to neuronal activation (Chang and Glover, 2009; Liu et al., 2013; Stefanovic et al., 2006). Specifically, reduced vascular responsiveness has been associated with reduced BOLD activation amplitude as well as a slowing down in the BOLD response dynamics (Behzadi and Liu, 2005; Liu et al., 2004; Rack-Gomer and Liu, 2012), setting the stage for our study of the effect of CVR on the rs-fMRI signal. Indeed, CVR is a major factor determining the hemodynamic response to neuronal activity, which in turn modulates rs-fcMRI signal amplitude (see review (Liu, 2013)). Specifically, the hemodynamic response determines the BOLD signal amplitude and subsequently the rs-fMRI BOLD signal-to-noise ratio (SNR); different signal SNRs will in turn lead to different connectivity measurements. Such biases may obscure the meaning of rs-fMRI functional connectivity measurements (Birn et al., 2006), which relies largely on temporal synchrony in BOLD signals. Nonetheless, the relationship between CVR and rs-fMRI functional connectivity has yet to be quantified in human fMRI data.

In this work, we aim to illustrate experimentally the relationship between CVR and rs-fMRI functional connectivity measurements through direct measurements in healthy adults. We modulate CVR within each subject by subtly altering the perceived “baseline” PETCO₂, and measure the result of such baseline alterations on rs-fcMRI. That is, CVR and rs-fcMRI were each measured at 3 matched vascular conditions, dictated by their associated PETCO₂ levels. In our previous work, we used this precise set up to modulate within-subject CVR (Halani et al., 2015). In this study, we build upon previous work to examine how rs-fcMRI measurements change as a result of altered CVR within and between subjects. We demonstrate (1) a significant positive relationship between CVR and rs-fMRI functional connectivity in the motor and executive-control networks, distinct from potential neuronal connectivity changes with CO₂; (2) this within-subject fcMRI–CVR relationship is highly variable across individuals.

Materials and methods

Participants

We studied 18 healthy participants, (10 men, 8 women), aged from 18 to 32 years (mean = 26.7 years, SD = 4.3). Participants were recruited through the Baycrest Participants Database, consisting of individuals from the Baycrest and local communities. The study was approved by the research ethics board (REB) of Baycrest, and the experiments were performed with the understanding and written consent of each participant, according to REB guidelines.

MRI acquisition

All images were acquired using a Siemens TIM Trio 3 Tesla System (Siemens, Erlangen, Germany). The scans employed 32-channel phased-array head coil reception and body-coil transmission. Resting-state BOLD fMRI data was acquired using a gradient-echo EPI pulse sequence (TR = 380 ms, TE = 30 ms, FA = 40°, 7 slices, 3.44 × 3.44 × 6.25 mm³, 950 volumes). BOLD-based CVR was measured using the second echo of a dual-echo pseudo-

continuous ASL (pCASL) sequence (TR = 3500 ms, TE_{BOLD} = 25 ms, FA = 90°, 20 slices, 3.44 × 3.44 × 6 mm³, 120 volumes). The pCASL data was also used in a separate publication concerning CVR measurement (Halani et al., 2015). During both the rs-fMRI and CVR scans, heart rate was monitored using the scanner's built-in finger oximeter, and respiration was monitored using a pressure-sensitive belt attached just below the ribcage. Moreover, a 2-minute motor-functional localizer (functional scout) was collected using gradient-echo EPI BOLD, during which the subject was instructed to perform 2 repetitions of a block-design bilateral finger apposition task (40 s ON–40 s OFF). Key scan parameters for the functional scout are: TR = 2 s, TE = 30 ms, voxel size = 3.5 × 3.5 × 5 mm³). The task-related region was the target region for the subsequent analyses to avoid the potential bias of respiratory tasks on motor connectivity in breathing-related motor regions. Moreover, a T₁-weighted MPRAGE anatomical image was acquired (TR = 2400 ms, TE = 2.43 ms, FOV = 256 mm, TI = 1000 ms, readout bandwidth = 180 Hz/px, voxel size = 1 × 1 × 1 mm³).

Vascular tension manipulations

All vascular manipulations were achieved by administering mixtures of O₂, CO₂ and medical air delivered using the RespirAct™ breathing circuit (Thornhill Research, Toronto, Canada), designed to provide computerized and independent targeting of end-tidal O₂ (PETO₂) and CO₂ (PETCO₂) pressure using the sequential gas delivery method (Slessarev et al., 2007). This method was chosen to maximize steady-state PETCO₂-targeting accuracy and stability while minimizing PETO₂ confounds during CO₂-based CVR measurements (Chen and Pike, 2010b; Halani et al., 2015; Mark et al., 2010; Prisman et al., 2008) and has demonstrated significant advantages over alternative methods (Mark et al., 2010; Tancredi and Hoge, 2013). We used this setup to achieve precise manipulations of basal PETCO₂ in each subject. Specifically, in addition to each subject's natural baseline (normocapnia), we also induced hypercapnic and hypocapnic baselines, which are both separated from the normocapnic baseline by 4 mm HgCO₂. Throughout the respiratory challenges, breath rate was self-regulated. The RespirAct™ device achieves hypocapnia mainly through increased breathing depths, and hypercapnia through upregulating the level of CO₂ in the air supply. The sequence of capnic conditions was varied in a pseudo-randomized manner across different subjects, with approximately 2 min between conditions. The breath-by-breath CO₂ levels were recorded at a rate of 50 Hz.

CVR and rs-fMRI measurements

For CVR measurement, 3 runs of dual-echo pCASL were performed. More specifically, PETCO₂ was sinusoidally modulated (Blockley et al., 2011) during the dual-echo pCASL scans at each of the 3 baseline PETCO₂ conditions, with a period of 120 s; 3 periods of sinusoidal PETCO₂ variations were induced with a baseline-to-peak amplitude of ±4 mm Hg, following a 1-minute baseline. This sinusoidal manipulation was applied at the 3 vascular-tension levels described earlier. The ordering of the different baselines was randomized to minimize biases. These mild PETCO₂ changes result in slight changes in the subject's vascular tension with negligible changes in cerebral oxidative metabolism, a potential confound for CO₂-based vascular assessment (Chen and Pike, 2010a). The experimental protocol is illustrated in detail in Fig. 1.

Likewise, rs-fMRI metrics including functional connectivity (fcMRI) were measured using the 3 runs of rs-fMRI scans (950 frames per run), each performed at a different vascular-tension level (hyper-, hypo-, and normocapnia). The hypo- and hypercapnic levels were also separated from normocapnia by 4 mm Hg CO₂, matching those of the CVR measurements. The rs-fMRI scans were performed immediately before the CVR scans, and the match between the rs-fMRI and CVR capnic levels was closely monitored during data acquisition and analysis.

Data analysis

Motor-cortex segmentation—Cortical tissue segmentation was performed using the FreeSurfer package (publicly available at: <http://surfer.nmr.mgh.harvard.edu>). The procedure includes brain extraction (Segonne et al., 2004), transformation into the MNI152 standard space, intensity normalization (Sled et al., 1998), tessellation of the gray matter white matter boundary, automated topology correction (Segonne et al., 2007), and surface deformation following intensity gradients to optimally place the gray/white and gray/CSF borders at the location where the greatest shift in intensity defines the transition to the other tissue class (Fischl and Dale, 2000). We extracted the primary motor cortical parcellation, segmented as Brodmann's Area 4 using an automated segmentation algorithm (Fischl et al., 2002), dilated by 1 mm in all 3 planes. This motor parcellation would help to confine our ROI to the primary motor region.

Functional data preprocessing—Functional images, including the tag and control images in the pCASL data, and T₁-weighted anatomical images were separately preprocessed using SPM8 (Wellcome Trust Centre for Neuroimaging, London, UK, (Friston et al., 1995)) and FSL (FMRIB Centre, Oxford). The first four time frames were discarded to ensure MR steady state. Preprocessing for functional images included retrospective head motion correction, slice-timing correction using sinc interpolation, spatial transformation into a Montreal Neurological Institute (MNI152) space, and spatial smoothing with a 6-mm full-width at half-maximum (FWHM) Gaussian kernel. We band-pass filtered the rs-fMRI data to the 0.008–0.09 Hz range. Note that due to our high sampling rate (TR = 0.38 s), we were able to directly filter out the fundamental cardiac and respiratory frequencies. However, we recognize that higher-order harmonics may remain, albeit their amplitudes should be much lower than that of the fundamental frequency peak. Thus, we also assessed whether cardiac and respiratory frequencies were altered by the capnic level used.

Anatomical images were co-registered with their corresponding realigned functional data and segmented into gray and white matter tissue probability maps using unified segmentation (Ashburner and Friston, 2005). Exploiting this anatomical information, we assume that the physiological noise contribution arising from low-frequency cardiac pulsation and respiration is globally distributed, and that the white matter and cerebrospinal fluid (CSF) could serve as noise regions-of-interest (ROIs). The first 6 principal components derived from the signal in the noise ROIs were then removed by projection onto the orthogonal complement of the range space of the noise regressors. In addition, we regressed out frame-by-frame motion (3 displacement and 3 rotational parameters as well as their first-order temporal derivatives).

Cerebrovascular reactivity—For the CVR calculation, the BOLD signal is calculated by averaging consecutive tag and control images from the second echo of the pCASL data. First, the CO₂-response delay in BOLD time course was accounted for at each voxel. This delay was estimated from the phase difference between the BOLD or CBF time courses and that of PETCO₂, enabling the alignment of the fMRI and PETCO₂ time series for maximal correlation. For this alignment, both PETCO₂ and fMRI data were upsampled to a common higher frequency, such that delays that are shorter than TR could be measured. Following the alignment, the PETCO₂ was interpolated to the pCASL TR and detrended at half the total duration of the respiratory paradigm. Outlier removal was performed based on Cook's distance from the initial linear model fit and the points with the Cook's distance greater than 4/N is discarded, where N is the number of time points (Bollen and Jackman, 1990). Subsequently, a linear model is fitted to the BOLD (dependent variable) and PETCO₂ (independent variable) values and CVR is defined as the slope of the linear model. The spatially specific CVR was thresholded at 0 to minimize biases introduced by noise. Additionally, we excluded data associated with spiking in PETCO₂ time course.

We computed the regional mean and standard deviation of the CVR estimates across each motor ROI. Specifically, in order to generate representative regional CVR values unbiased by outliers, we first removed outlier voxels from each ROI using the non-parametric algorithm based on the Tukey's box-plot method (Patterson, 2012; Tukey, 1977); this method suits the present application as it does not assume a normal distribution for the voxel-wise CVR values.

Resting-state measurements—As mentioned earlier, the motor network is known for its robustness and simplicity. Due to our desire to sample quickly, our rs-fMRI acquisition was based on partial brain coverage. Thus, in addition to the motor network, the only other network we have access to is the executive-control network. In terms of functional connectivity, we generated rs-fcMRI maps using a seed-based analysis approach. Our seed-selection procedures are summarized in Table 2. All preprocessed images were transformed into MNI152 space. The denoised and band-pass filtered data were used to compute bilateral connectivity.

For probing the motor network, seeds were defined on a per-subject basis, as the overlap between the functional scout region of interest and the primary motor anatomical segmentation (Brodmann's Area 4). Moreover, ipsilateral functional connectivity values were computed based on the contralateral seed. That is, correlation maps were first computed using the left-motor seed, with the correlation values in the seed region disregarded through masking. Then, a similar procedure is performed, but using the right-motor seed. The two hemispheric connectivity maps were then summed to form bilateral motor rs-fcMRI maps. This approach allowed us to minimize autocorrelation-related biases (Arbabshirani et al., 2014).

For the executive-control network, maps were generated from 2 seeds in each hemisphere, and subsequently averaged across hemispheres to create a whole-brain connectivity map. That is, as the executive-control network was not associated with a well-defined anatomical parcellation, we opted to construct the seeds as 6 mm spheres in MNI152 space, centred at

the centroids of the superior-frontal and superior-parietal nodes, as defined by the 1000-brain fcMRI atlas published by Yeo et al. (2011). Furthermore, left- and right control networks were first mapped separately based on left and right seeds, with the seed regions discarded from each intermediate connectivity map prior to the cross-hemisphere averaging. Finally, connectivity was computed as a regression coefficient using the CONN Toolbox (MIT, publicly available at <https://www.nitrc.org/projects/conn/>).

In addition, given prior literature on the relationship between CVR and the resting-state fMRI signal fluctuation amplitude, we also computed the amplitude of low-frequency fluctuations (ALFF) (Di et al., 2013). The ALFF was computed as the sum of the Fourier power spectrum of the post-processed rs-fMRI time series (that matches with the data used in the functional connectivity computations) normalized to the mean BOLD signal intensity.

Region-of-interest definition—We focused our analysis on the motor network and the executive-control network. We specifically localized the hand area of the motor network to avoid CO₂-related confounds. For both networks, we customized the region of interest (ROI) for each subject.

Motor-network ROI: Based on the motor scout, a *t*-map was generated and thresholded at a *p* < 0.05 level of significance (corrected for cluster size). This region was then overlapped with the FreeSurfer segmentation of primary motor cortex customized to each subject's native space in order to remove potential false activations elsewhere in the cortex. The conjunction between the two was then overlapped with the functional connectivity map obtained at normocapnic baseline, and thresholded to retain only positive correlation values. The same ROI is then used for all three vascular conditions, as we wished to avoid vascular-condition related ROI-size variations, and aimed to simply compare the strengths of network connectivity. A sample illustration of the motor-network ROI definition is shown in Fig. 2.

Executive-control network ROI: For assessing fcMRI, ALFF and CVR in the executive-control network, we defined an ROI in standard (MNI) space based on the overlap between the 1000-brain functional atlas (mentioned earlier) and the seed-based functional connectivity map. The average ROI fcMRI values were computed after excluding values from the seed regions themselves. This ROI is then translated into each subject's native space for assessing regional CVR.

Statistical analyses—We averaged our voxel-wise CVR and rs-fMRI measures within the aforementioned ROIs, and assessed their dependence on basal capnic level (i.e. hypo-, normo- and hypercapnia), each representing a different level of vascular tension. The significance of any effects was assessed using repeated-measures ANOVA. We also quantified this vascular-state dependence across subjects using a linear regression model, in which the line fits were based on least-squares minimization, and weighted by variability on both the ordinate and the abscissa. These relationships were quantified when averaging across all vascular (capnic) conditions to allow a more cross-subject assessment, but also at each capnic condition separately, to allow a comparison of CVR effects in different vascular conditions. Differences between regressions across capnic conditions were assessed using the analysis of covariance (ANCOVA).

In view of potential inter-subject variability in the observed effects, we further performed linear mixed effects analyses (see Supplementary Materials for details). Moreover, we performed mediation analyses to assess the relationship amongst the “independent” variables in the mixed-effects models.

Results

Two subjects were excluded from the analysis due to excessive head motion (consistently beyond 1 mm). In addition, we removed an outlier, yielding a total of $N = 15$ subjects. In Fig. 3 we summarize the $PETCO_2$ and $PETO_2$ levels achieved during the three capnic levels. As expected, while the $PETCO_2$ level is significantly different between capnic conditions, $PETO_2$ alterations are negligible. In addition, there is no significant difference between average $PETCO_2$ levels associated with the rs-fMRI and CVR data-acquisitions for similar capnic conditions. Moreover, in Table 1, we report physiological and motion parameters for all three conditions. Heart and respiratory rates were estimated from the physiological logs recorded during the scans, while motion parameters were estimated using the FSL FEAT. Our records show no significant difference across capnic conditions in any of the listed parameters.

Group-average CVR and functional connectivity maps in the motor network are shown in Fig. 4, demonstrating subtle spatial-extent differences in motor-connectivity patterns across the three vascular (capnic) conditions. In Fig. 5, we examine the vascular-state dependence of individual measures in the motor-network ROI. One-way repeated-measures ANOVA results are summarized in Table 3. The ANOVA returned significant baseline-associated differences in CVR estimates in the motor network ($p = 0.05$), but not in the executive-control network ($p = 0.11$), although similar CVR trends are seen in both networks (Figs. 5a & b). However, rs-fcMRI and BOLD signal amplitude (ALFF) measurements were generally not significantly dependent on the capnia factor (i.e. hypo-, normo- and hypercapnia), as per the ANOVA. Interestingly, in the control network (Fig. 5b), ALFF and CVR shared a similar trend of being highest at normocapnia. However, this was not the case with fcMRI, which peaked at hypocapnia.

To further investigate the association between CVR and functional connectivity, we plotted connectivity strength versus CVR for different subjects and capnic conditions (Fig. 6a, 15 subjects, each with three capnic conditions). We present a fit to the inter-capnia averages in Figs. 6, 7 and 8, with different colors representing different subjects. The motor-ROI functional connectivity values were found to be significantly associated with CVR (Fig. 6a), characterized by a slope of 1.51, $r^2 = 0.30$ and $p = 0.036$. The significant CVR dependence remained when the plot was repeated at the normo- and hypercapnic baselines, but not during hypocapnia (Fig. 6b). For the control network, while the average values (across 3 capnic conditions) resulted in a significant positive relationship between CVR and fcMRI (Fig. 3c, $p = 0.049$), it was not the case when each capnic condition was examined separately (Fig. 6d). Nonetheless, ANCOVA results ($p = 0.77$ and 0.99) suggest no difference between the regressions at the different capnic conditions.

As mentioned earlier, the inclusion of ALFF in the investigation was driven by its potential mediating role between CVR and fcMRI measures. When all participants and conditions were taken into account, ALFF was not significantly associated with rs-fMRI functional connectivity values in any of our network ROIs (Figs. 7a–d). There was no significant difference between the rs-fcMRI and ALFF measurements across the various capnic conditions for either of the networks (ANCOVA: $p = 0.91$ and 0.31 for motor and control network, respectively). Nonetheless, ALFF and CVR were significantly associated at normo- and hypercapnia in the motor and control networks (Figs. 8b & d), in agreement with average results shown in Figs. 8a and c. Again, there was no difference in the relationships across capnic conditions (ANCOVA: $p = 0.64$ and 0.65 for motor and control networks, respectively). We note that as we intended to perform the fits in Figs. 7 and 8 using the same subjects included in the fcMRI–CVR fit, thus we did not perform outlier removal in producing these two sets of plots.

To test whether the weaker fcMRI–CVR associations in the control network is due to the inclusion of more heterogeneous regions in the ROI, we repeated the analysis in the frontal and parietal components of the network separately. Results in Fig. 9 show that fcMRI values in the frontal control network demonstrate much stronger CVR-dependence than in the parietal control network.

Despite motion correction and the regression of motion parameters, we found the ALFF to be significantly correlated with mean frame-to-frame head motion (motor: $p = 0.00037$, $r^2 = 0.64$; executive control: $p = 0.0072$, $r^2 = 0.41$). This was not the case between CVR and head motion (motor: $p = 0.082$, $r^2 = 0.22$; control: $p = 0.55$, $r^2 = 0.027$), neither was it between functional connectivity and head motion (motor: $p = 0.66$, $r^2 = 0.01$; control: $p = 0.21$, $r^2 = 0.11$). Thus, we regressed out mean head motion from the ALFF when a significant motion effect was found, and re-evaluated the ALFF–CVR and fcMRI–ALFF relationships. The ALFF–CVR regression remained significant (motor: $p = 0.012$, $r^2 = 0.39$; control: $p = 0.01$, $r^2 = 0.38$). As well, the fcMRI–ALFF relationship remained insignificant (motor: $p = 0.24$, $r^2 = 0.1$; control: $p = 0.85$, $r^2 = 0.0028$). The results are illustrated in Fig. S1 (Supplementary materials).

Furthermore, we constructed linear mixed-effects models to address the within and between-subject structures of CVR, ALFF and capnic condition. The methods and results (Table S1) are included in the Supplementary materials. None of the modeled effects was significant, potentially due to high variability given our limited sample size, as illustrated in Fig. S2 (Supplementary Materials). However, when considering inter-subject variability as a random effect, ALFF had the strongest potential fixed effect on fcMRI estimates in the motor network ($p = 0.10$). Finally, our mediation analysis did not reveal ALFF as a significant factor mediating the relationship between CVR and fcMRI measurements (Table S2, Supplementary materials).

Discussion

CVR is commonly thought to be a biomechanical trait (Kastrup et al., 1998, 1997) of the vasculature that is not directly related to functional networks. However, in this work, we

have shown that CVR is significantly and positively associated with resting-state functional connectivity measurements across individuals. Nonetheless, this relationship was highly variable amongst individuals. To minimize potential neuronal influences of CO₂ (Peng et al., 2013; Yuan et al., 2013), we primarily focus on the bilateral hand areas of the motor cortex, as was done in the seminal work by Biswal et al. (1995), and the bilateral executive-control network, another prominent rs-fMRI network. Within the confines of our brain coverage, we also examined the executive-control network to test the generalizability of our findings.

The association between CVR and resting-state fMRI connectivity

In accordance with our hypothesis, the first key finding of this work is that rs-fMRI functional connectivity is significantly associated with CVR. Given the bipolar (up and down) nature of intrinsic brain activity, we felt that a bipolar CO₂ stimulus (instead of the conventional block-design hypercapnic stimulus) better emulates any potential influence that CVR may have on resting-state fMRI fluctuations in the context of rs-fMRI applications. Furthermore, while there are alternative ways of measuring CVR, in particular using cerebral blood flow (Halani et al., 2015; Tancredi et al., 2012), our choice of gradient-echo BOLD for CVR measurement is also motivated by the desire to assess BOLD-specific fcMRI associations with BOLD-specific CVR. Our results demonstrate that both hypercapnic and hypocapnic states are associated with decreased CVR. This effect is described in detail in our recent work (Halani et al., 2015), and is in agreement with previous results derived from microsphere-enhanced electromagnetic flowmetry (Lopez de Pablo et al., 1982), Doppler ultrasound (Battisti-Charbonney et al., 2011; Carrera et al., 2011) and MRI (Sicard et al., 2003).

The capnic-level dependences of CVR and fcMRI values differed, indicating that basal capnic condition (hypocapnia vs. normocapnia vs. hypercapnia) affects CVR and fcMRI in distinct ways (Fig. 5). Across the group, rs-fMRI functional connectivity of the motor network also depend significantly on the baseline capnic state, with the hypocapnic baseline associated with the highest connectivity values, and hypercapnic baseline associated with the lowest connectivity. The latter finding is in agreement with early data from Biswal (Biswal et al., 1997). This association, however, is not consistent across the brain, as rs-fMRI connectivity of executive control network, specifically in the parietal regions, is not sensitive to capnic state.

The most obvious explanation for the vascular contribution to the lower fcMRI values at hypercapnia is outlined in the Introduction section. Specifically, significant basal vasodilation or constriction induced by our experimental design may shift the BOLD–PETCO₂ curve into the sublinear regime, as can be predicted using Eq. (1) (Hoge et al., 1999). Thus, during the hypercapnic state, for instance, the sensitivity of BOLD signal to neuronal fluctuations may be reduced compared to those at normocapnia. Consequently a proportionately larger fraction of the BOLD signal fluctuations could be attributed to noise and artifacts (Liu, 2013), resulting in lower neurosensitivity and hence reduced ability to detect functional connectivity, as outlined by Biswal et al. (1997). It is notable that such a dependence of rs-fMRI connectivity on CVR is observed even in our group of young healthy adults with no known neuronal or vascular dysfunction.

An alternate explanation relates to the dynamic features of the hemodynamic response function, and in turn, its implications in fMRI computations. The hemodynamic response function (HRF) characterizes the link between the BOLD signal and neuronal activity, with CVR representing its magnitude alone. We note that the dynamics of the HRF is likely altered by changes in baseline vascular conditions; in fact, we have previously reported that the CO₂-related HRF at hypercapnic baseline is significantly slower than at normocapnic baseline (Halani et al., 2015). Should these HRF changes vary between the left and right motor cortices, for instance, a reduction in correlation-based connectivity may occur. Such a mechanism would be analogous to previously reported caffeine-induced motor connectivity reduction (Rack-Gomer and Liu, 2012). To probe this possibility, we assessed the locations of the centroids of the Fourier spectra of the post-processed rs-fMRI time courses. At hypo-, normo- and hypercapnia, the group-average centroids in grey matter are at 0.080 ± 0.051 , 0.078 ± 0.053 and 0.086 ± 0.063 Hz, respectively, not significantly different from one another. Similar results apply to the white matter (0.087 ± 0.066 , 0.090 ± 0.059 and 0.099 ± 0.074 Hz, respectively, for the three capnic conditions). Nonetheless, these measurements may lack the sensitivity to detect the hypothesized HRF changes in the resting state. In this study, we focus on the CVR aspect of the HRF but not its dynamics, which constitutes a potential limitation and area for future efforts.

As revealed by the scatter plots, the inter-subject variation of CVR is positively and significantly correlated with those in rs-fMRI for both the motor and control networks (Fig. 6). While the statistical significance of the regression lines varied between vascular states, our ANCOVA results indicated no significant difference in the fMRI-CVR regression lines across vascular states. Thus, our results suggest that the fMRI-CVR relationship is not dependent on capnic level, at least within the conditions examined in this study. Experimentally, we noticed a higher inter-subject variability in the physiological response to hypocapnia than to the other two states, which may have resulted in a less consistent fMRI-CVR relationship across subjects at this state. Lastly, the distinct CVR dependences in the frontal and parietal portions of the control network (Fig. 9) highlight the spatial heterogeneity of the CVR dependence.

Overall, our findings demonstrate experimentally, for the first time, the vascular modulation of functional connectivity measurements, specifically due to CVR, even within a relative narrow range of CVR values, taken from healthy young adults. These findings are consistent with recent discoveries of vascular-neural interplays in fMRI (Bright and Murphy, 2015; Tong et al., 2015). However, the discrepancy between the CVR and fMRI trends observed in Fig. 5 points to a secondary mechanism for the observed fMRI dependence of basal capnic state, as will be described later. However, based on our findings, we do not believe that the CVR bias in fMRI measurements can be corrected based on a single linear relationship, but would depend on individual CVR and resting PETCO₂ measurements as well as the network being considered.

The role of BOLD signal amplitude

The BOLD fluctuation amplitude has been previously found to explain a significant portion of the vascular reactivity variability seen across subjects (Kannurpatti et al., 2014, 2010,

2011). Moreover, the BOLD fluctuation has been found to correlate with inter-subject variability of the network connectivity strength (Di et al., 2013), although the effect was not found in all functional network regions. Thus, given the bridging role of BOLD fluctuation amplitude between CVR and fcMRI measurements, we were compelled to assess the involvement of ALFF in the observed fcMRI–CVR relationship.

As an analogy from task-based BOLD, previous studies reported reduced BOLD signal amplitude in response to evoked task-related activation during hypercapnic states (Stefanovic et al., 2006), and the opposite for hypocapnia (Cohen et al., 2002). Hypercapnia is a vasodilatory challenge and increases the basal CBF, which in turn would increase blood oxygenation. Such increases were found to result in reduced BOLD responsiveness to neuronal activity, as demonstrated in previous task-based findings that have shown that stimulus evoked BOLD signal amplitude reduces during hypercapnia (Stefanovic et al., 2006).

It is interesting to note that while the resting capnic condition affects both ALFF and fcMRI, the group-level trends shown in Fig. 5 are different for the two. This discrepancy seems to indicate that ALFF is more closely related to CVR than is fcMRI, suggesting that the CVR effect on fcMRI is likely mediated by the ALFF. Such a finding is also consistent with previous findings regarding the resting-state fluctuation amplitude (RSFA) metric (Kannurpatti and Biswal, 2008; Kannurpatti et al., 2014). However, in a separately mediation analysis (Supplementary materials, Table 2S), we did not observe a significant mediating effect, potentially due to the limited group size. This is also a likely indication that the ALFF (and by extension, RSFA) encompasses both purely vascular as well as neurovascular fluctuations, and is thus more complex than CVR or task-evoked fMRI responses. This point may underlie the seemingly paradoxical observation that the ALFF is not significantly correlated with rs-fcMRI scores (Fig. 7) despite the strong ALFF–CVR relationship, in that the neuronal contributions to ALFF and rs-fcMRI may be influenced by vascular states in distinct manners.

We note that despite frame-by-frame motion correction and regression in rs-fMRI preprocessing, group-level motion effects in ALFF values remained. While the potential biases introduced by frame-by-frame motion regression (Fox et al., 2009; Power et al., 2012) will remain a limitation in this work, we feel that our subsequent regression to remove motion effect at the group level enhanced the robustness of our findings.

Potential metabolic involvement

In this work, we modulated PETCO₂ while keeping PETO₂ constant in awake and free-breathing humans. While we demonstrated a significant role of CVR in the dependence of fcMRI measurement on CO₂-mediated vascular tension, there may be other mechanisms underlying this fcMRI variability. Despite our choice of low levels of PETCO₂ manipulations, which were based on the premise of global iso-metabolism (Chen and Pike, 2010a; Jain et al., 2011), we recognize that CO₂ may have subject-dependent metabolic implications that induce changes in functional connectivity. Indeed, our observation of reduced motor rs-fcMRI measurements with elevated PETCO₂ (Fig. 5a) are in agreement with findings by Xu et al. (Xu et al., 2011). This was attributed to reduced alpha-wave

amplitude, consistent with previous findings using intracortical recordings and magnetoencephalography during hypercapnia or carbogen-inhalation (Hall et al., 2011; Thesen et al., 2011; Zappe et al., 2008). Similar electroencephalography (EEG) power reductions in isoflurane-anesthetized rats and inter-hemispheric coherence increases were reported in the somatosensory cortex using intracortical recordings (Nasrallah et al., 2015). More recently, multi-spectral rhythms have been found to decrease with increasing PETCO₂ in a linear fashion (Driver et al., 2015), prompting further experiments to study the neurovascular implications of CO₂. However, while Nasrallah et al. reported an increased EEG signal correlations with increasing CO₂ in the 0.04–0.07 Hz range, we did not observe corresponding fcMRI increases, potentially due to the use of isoflurane anesthesia by Nasrallah et al.

In this work, we extend the experimental scope of previous studies to the hypocapnic state, and find that the same trend applies, as fcMRI measurements are higher at hypocapnic compared to normocapnic and hypercapnic baselines in the motor network. While previous work on the topic by Xu et al. (2011) focused on the default-mode network and attributed the reduced connectivity at hypercapnia to arousal effects, we note that the default-mode network is unique in many ways and may not offer the generalizable insight into biophysical interplays. In that regard, our concordant finding in the motor network brings into focus the possibility that CO₂ affects functional connectivity at a broader scale, and not purely through arousal or vigilance alterations. Indeed, as our participants underwent similar respiratory exercises for all three capnic conditions (the only variation being actual PETCO₂ levels), their levels of arousal is unlikely to vary with capnic state. However, CO₂ did not impact the executive-control network as strongly as it did in the motor network, highlighting the spatial heterogeneity in the effect of CO₂ on fcMRI measures. This argument is bolstered by observed heterogeneity between the fcMRI–CVR relationships in the frontal and parietal control networks (Fig. 9). A potential explanation for this finding can be gleaned from simulation results by Liu et al. (Liu, 2013), in which the dependence of functional connectivity measurements on vascular modulation is likely to depend on the fMRI contrast-to-noise ratio (CNR). The CNR, in turn, is determined in part by the physiological parameters that contribute to the strength of the underlying true BOLD signal, as shown in the BOLD equation. Specifically, given a fixed CMRO₂ pattern, an increasing CVR and in baseline CBF (CBF₀) would both result in an increase in the amplitude of the true BOLD signal, as shown in Eqs. (1)–(2). To speak to that point, the motor and superior-frontal (part of frontal control network) regions are amongst the most highly perfused (with high CBF₀) across the cortical mantle (Chen et al., 2011), potentially enhancing our ability to detect vascular modulation of BOLD functional connectivity in these regions.

When comparing our findings to electrophysiological measurements, using intracortical recordings, Nasrallah et al. observed an increase in bilateral motor connectivity (via coherence) during hypercapnia (Nasrallah et al., 2015), which seems to contradict the fMRI findings — we attribute this seeming discrepancy to the involvement of CVR. Thus, potential metabolic effect of CO₂ may complement the effect of CVR on fcMRI, and may be mediated by the positive relationship between neuronal activity amplitude and BOLD amplitude, and in turn, the relationship between the latter and BOLD sensitivity in the

presence of noise. In this regard, it is interesting to note that CVR and neural metabolism likely both contribute to the sensitivity of BOLD functional connectivity to resting CO₂.

Inter-subject variability in the CVR dependence on basal CO₂

Our original experimental hypothesis was based on the assumption that a deviation from normocapnia, either in the form of hypercapnia or hypocapnia, would result in some degree of reduced vasoreactivity to a bipolar vascular stimulus. Although we observed this trend at a group level, this was not the case for each individual subject. Interestingly, the relationship between CVR and the underlying vascular tension was highly variable across subjects. This vast inter-subject variability in vascular response was reflected in the inter-subject variability in vascular-tension dependence of functional connectivity values. However, as mentioned earlier, this variability may also be attributable to potential metabolic implications of elevated or reduced PETCO₂ (Xu et al., 2011), and its neurovascular consequences.

Potential caveats and future directions

In this work, we focused on two networks, due to our limited brain coverage (to achieve a TR of 380 ms). Thus, we were confined to the superior portion of the executive-control network (illustrated in Fig. 3). Also, we opted for a seed-based approach to compute functional connectivity for its simplicity and usefulness in explaining mechanisms (Biswal et al., 1995; Puce et al., 1995). However, we see our results relevant to measurements by other mainstay methods such as independent-component analysis (ICA), as ICA sensitivity to functional networks is also dependent on the BOLD SNR (Beckmann and Smith, 2004).

In addition, while we minimized the time elapsed between our CVR and rs-fMRI scans to the best of our abilities (mean separation between scans = 13 min), the fact that these data were not acquired simultaneously presents a potential source of confound. We attempted to control such a confound by strictly regulating the PETCO₂ agreement in the CVR–fcMRI scan pairs, but other time-related neural factors beyond our control may have contributed to the variability in the inter-subject CVR–fcMRI relationship.

The use of a very short rs-fMRI TR (0.38 s) raises the possibility of in-flow effects, which may remain despite our use of a low flip angle. In EPI BOLD imaging, inflow effects are more pronounced near major arteries and veins, and less at sites of small vessels (Gao and Liu, 2012). Flow patterns in these large vessels would be primarily driven by the cardiac and respiratory-sinus arrhythmic cycles, and in our case, may have been affected by higher harmonics of the cardiac oscillation. Although we recognize that these macrovascular flow effects would be much less pronounced when using conventional TRs (1–2 s), we do not expect the current results to be driven by potential inflow effects, as we did not observe any significant association between cardiac rate and the ALFF (MN: $p = 0.99$; ECN: $p = 0.87$).

We excluded the study of negative correlations from this study, mainly due to methodological limitations. Although negative correlations have been rather controversial and their observation has been less consistent than the positive correlations (Murphy et al., 2009), recent research has re-established their biological relevance (Carbonell et al., 2011; Chai et al., 2012). Within our methodology, however, the definition of negatively correlated

network ROIs at a group level is impeded by their lack of consistency, but will constitute a focus of future efforts.

Furthermore, in this work, we focus primarily on the influence of quantitative CVR on fcMRI measurements, in the context of modulated basal CO₂ levels. The dynamics of the vascular response also has important bearings on functional-connectivity measurements, and warrants follow-up investigation. Furthermore, we recognize that, given the potential entanglement of neural and vascular activity (Bright and Murphy, 2015; Tong et al., 2015), a more complete understanding of our observations regarding CVR would require the involvement of neurophysiological or metabolic measurements. Thus, our future work will involve techniques such as whole-brain MR oximetry (Chen and Pike, 2010a; Lu et al., 2012) and electroencephalography to more comprehensively examine the physiological modulators of rs-fMRI functional connectivity. In addition, given the strong significance of the CVR-related bias on fcMRI seen even in a group of young healthy adults, we will examine the implications of CVR on functional connectivity in older adult and adults with vascular risk.

Conclusion

Although cerebrovascular reactivity (CVR) is generally considered a biomechanical trait of the vasculature, it has a significant impact on fMRI-based functional connectivity measurements. In this work, we report a strong positive association between CVR and resting-state fcMRI measurements in healthy young adults, who have no known vascular or functional impairment. In addition, we demonstrate, for the first time, the magnitude and spatial consistency of this association, which are non-trivial and may have important implications for the sensitivity, reproducibility and interpretability of fcMRI measurements. Furthermore, our work highlights the vast inter-subject variability of the CVR–fcMRI relationship, suggesting the need for more detailed assessment of systemic physiological factors and their impact of rs-fMRI measurements.

Supplementary Material

Refer to Web version on PubMed Central for supplementary material.

Acknowledgments

This research was supported by the Natural Sciences and Engineering Council of Canada (NSERC App. 418443, JJC), the Canadian Institutes of Health Research (CIHR: App. 286286, JJC) and the Heart and Stroke Foundation Centre for Stroke Recovery (J. B. Kwinta). We thank Drs. Danny J. Wang and Lirong Yan from the University of California at Los Angeles for the dual-echo pCASL sequence, as well as Ms. Olivia Pucci and Dr. Joseph Fisher from the University of Toronto Health Network for help in the respiratory circuitry setup. Lastly, we thank Mr. Mohsin Kazmi for assisting with participant recruitment.

References

- Arbabshirani MR, Damaraju E, Phlypo R, Plis S, Allen E, Ma S, et al. Impact of autocorrelation on functional connectivity. *NeuroImage*. 2014; 102:294–308. [PubMed: 25072392]
- Ashburner J, Friston KJ. Unified segmentation. *NeuroImage*. 2005; 26:839–851. [PubMed: 15955494]

- Battisti-Charbonney A, Fisher J, Duffin J. The cerebrovascular response to carbon dioxide in humans. *J Physiol.* 2011; 589:3039–3048. [PubMed: 21521758]
- Beckmann CF, Smith SM. Probabilistic independent component analysis for functional magnetic resonance imaging. *IEEE Trans Med Imaging.* 2004; 23:137–152. [PubMed: 14964560]
- Behzadi Y, Liu TT. An arteriolar compliance model of the cerebral blood flow response to neural stimulus. *NeuroImage.* 2005; 25:1100–1111. [PubMed: 15850728]
- Birn RM, Diamond JB, Smith MA, Bandettini PA. Separating respiratory-variation-related fluctuations from neuronal-activity-related fluctuations in fMRI. *NeuroImage.* 2006; 31:1536–1548. [PubMed: 16632379]
- Birn RM, Cornejo MD, Molloy EK, Patriat R, Meier TB, Kirk GR, et al. The influence of physiological noise correction on test-retest reliability of resting-state functional connectivity. *Brain Connect.* 2014; 4:511–522. [PubMed: 25112809]
- Biswal BB, Kannurpatti SS. Resting-state functional connectivity in animal models: modulations by exsanguination. *Methods Mol Biol.* 2009; 489:255–274. [PubMed: 18839096]
- Biswal B, Yetkin FZ, Haughton VM, Hyde JS. Functional connectivity in the motor cortex of resting human brain using echo-planar. *Magn Reson Med.* 1995; 34:537–541. [PubMed: 8524021]
- Biswal B, Hudetz AG, Yetkin FZ, Haughton VM, Hyde JS. Hypercapnia reversibly suppresses low-frequency fluctuations in the human motor cortex during rest using echo-planar MRI. *J Cereb Blood Flow Metab.* 1997; 17:301–308. [PubMed: 9119903]
- Biswal BB, Kannurpatti SS, Rypma B. Hemodynamic scaling of fMRI-BOLD signal: validation of low-frequency spectral amplitude as a scalability factor. *Magn Reson Imaging.* 2007; 25:1358–1369. [PubMed: 17482411]
- Blockley NP, Driver ID, Francis ST, Fisher JA, Gowland PA. An improved method for acquiring cerebrovascular reactivity maps. *Magn Reson Med.* 2011; 65:1278–1286. [PubMed: 21500256]
- Bollen, KA., Jackman, RW. *Modern Methods of Data Analysis.* Sage; Newbury Park, CA: 1990. p. 257-291.
- Bright MG, Murphy K. Is fMRI “noise” really noise? Resting state nuisance regressors remove variance with network structure. *NeuroImage.* 2015; 114:158–169. [PubMed: 25862264]
- Carbonell F, Bellec P, Shmuel A. Global and system-specific resting-state fMRI fluctuations are uncorrelated: principal component analysis reveals anti-correlated networks. *Brain Connect.* 2011; 1:496–510. [PubMed: 22444074]
- Carrera E, Kim DJ, Castellani G, Zweifel C, Smielewski P, Pickard JD, et al. Effect of hyper- and hypocapnia on cerebral arterial compliance in normal subjects. *J Neuroimaging.* 2011; 21:121–125. [PubMed: 19888933]
- Carusone LM, Srinivasan J, Gitelman DR, Mesulam M-M, Parrish TB. Hemodynamic response changes in cerebrovascular disease: implications for functional MR imaging. *AJNR Am J Neuroradiol.* 2002; 23:1222–1228. [PubMed: 12169483]
- Chai XJ, Castañón AN, Ongür D, Whitfield-Gabrieli S. Anticorrelations in resting state networks without global signal regression. *NeuroImage.* 2012; 59:1420–1428. [PubMed: 21889994]
- Chang C, Glover GH. Relationship between respiration, end-tidal CO₂, and BOLD signals in resting-state fMRI. *NeuroImage.* 2009; 47:1381–1393. [PubMed: 19393322]
- Chen JJ, Pike GB. Global cerebral oxidative metabolism during hypercapnia and hypocapnia in humans: implications for BOLD fMRI. *J Cereb Blood Flow Metab.* 2010a; 30:1094–1099. [PubMed: 20372169]
- Chen JJ, Pike GB. MRI measurement of the BOLD-specific flow-volume relationship during hypercapnia and hypocapnia in humans. *NeuroImage.* 2010b; 53:383–391. [PubMed: 20624474]
- Chen JJ, Rosas HD, Salat DH. Age-associated reductions in cerebral blood flow are independent from regional atrophy. *NeuroImage.* 2011; 55(2):468–478. [PubMed: 21167947]
- Cohen ER, Ugurbil K, Kim SG. Effect of basal conditions on the magnitude and dynamics of the blood oxygenation level-dependent fMRI response. *J Cereb Blood Flow Metab.* 2002; 22:1042–1053. [PubMed: 12218410]
- Davis TL, Kwong KK, Weisskoff RM, Rosen BR. Calibrated functional MRI: mapping the dynamics of oxidative metabolism. *Proc Natl Acad Sci U S A.* 1998; 95:1834–1839. [PubMed: 9465103]

- Di X, Kim EH, Huang CC, Tsai SJ, Lin CP, Biswal BB. The influence of the amplitude of low-frequency fluctuations on resting-state functional connectivity. *Front Hum Neurosci.* 2013; 7:118. [PubMed: 23565090]
- Driver ID, Whittaker J, Bright MG, Muthukumaraswamy SD, Murphy K. Linear dependence of neuronal oscillations on hypercapnia level: implications for CO₂ calibrated fMRI. *Int Soc Magn Reson Med, Toronto.* 2015:2132.
- Fischl B, Dale AM. Measuring the thickness of the human cerebral cortex from magnetic resonance images. *Proc Natl Acad Sci U S A.* 2000; 97:11050–11055. [PubMed: 10984517]
- Fischl B, Salat DH, Busa E, Albert M, Dieterich M, Haselgrove C, et al. Whole brain segmentation: automated labeling of neuroanatomical structures in the human brain. *Neuron.* 2002; 33:341–355. [PubMed: 11832223]
- Fox MD, Zhang D, Snyder AZ, Raichle ME. The global signal and observed anticorrelated resting state brain networks. *J Neurophysiol.* 2009; 101:3270–3283. [PubMed: 19339462]
- Friston KJ, Holmes AP, Worsley KJ, Poline J-B, Frith CD, Frackowiak RSJ. Statistical parametric maps in functional imaging: a general linear approach. *Hum Brain Mapp.* 1995; 2:189–210.
- Gao JH, Liu HL. Inflow effects on functional MRI. *NeuroImage.* 2012; 62:1035–1039. [PubMed: 22019882]
- Halani S, Kwinta JB, Golestani AM, Khatamian YB, Chen JJ. Comparing cere-brovascular reactivity measured using BOLD and cerebral blood flow MRI: the effect of basal vascular tension on vasodilatory and vasoconstrictive reactivity. *NeuroImage.* 2015; 110:110–123. [PubMed: 25655446]
- Hall EL, Driver ID, Croal PL, Francis ST, Gowland PA, Morris PG, et al. The effect of hypercapnia on resting and stimulus induced MEG signals. *NeuroImage.* 2011; 58:1034–1043. [PubMed: 21762783]
- Hoge RD, Atkinson J, Gill B, Crelier GR, Marrett S, Pike GB. Investigation of BOLD signal dependence on cerebral blood flow and oxygen consumption: the deoxyhemoglobin dilution model. *Magn Reson Med.* 1999; 42:849–863. [PubMed: 10542343]
- Jain V, Langham MC, Floyd TF, Jain G, Magland JF, Wehrli FW. Rapid magnetic resonance measurement of global cerebral metabolic rate of oxygen consumption in humans during rest and hypercapnia. *J Cereb Blood Flow Metab.* 2011; 31:1504–1512. [PubMed: 21505481]
- Kannurpatti SS, Biswal BB. Detection and scaling of task-induced fMRI-BOLD response using resting state fluctuations. *NeuroImage.* 2008; 40:1567–1574. [PubMed: 18343159]
- Kannurpatti SS, Biswal BB, Kim YR, Rosen BR. Spatio-temporal characteristics of low-frequency BOLD signal fluctuations in isoflurane-anesthetized rat brain. *NeuroImage.* 2008; 40:1738–1747. [PubMed: 18339559]
- Kannurpatti SS, Motes MA, Rypma B, Biswal BB. Neural and vascular variability and the fMRI-BOLD response in normal aging. *Magn Reson Imaging.* 2010; 28:466–476. [PubMed: 20117893]
- Kannurpatti SS, Motes MA, Biswal BB, Rypma B. Assessment of unconstrained cerebrovascular reactivity marker for large age-range FMRI studies. *PLoS One.* 2014; 9:e88751. [PubMed: 24551151]
- Kastrup A, Dichgans J, Niemeier M, Schabet M. Changes of cerebrovascular CO₂ reactivity during normal aging. *Stroke.* 1998; 29:1311–1314. [PubMed: 9660378]
- Leopold DA, Maier A. Ongoing physiological processes in the cerebral cortex. *NeuroImage.* 2012; 62:2190–2200. [PubMed: 22040739]
- Liu TT. Neurovascular factors in resting-state functional MRI. *NeuroImage.* 2013; 80:339–348. [PubMed: 23644003]
- Liu TT, Behzadi Y, Restom K, Uludag K, Lu K, Buracas GT, et al. Caffeine alters the temporal dynamics of the visual BOLD response. *NeuroImage.* 2004; 23:1402–1413. [PubMed: 15589104]
- Liu P, Hebrank AC, Rodrigue KM, Kennedy KM, Park DC, Lu H. A comparison of physiologic modulators of fMRI signals. *Hum Brain Mapp.* 2013; 34:2078–2088. [PubMed: 22461234]
- Lopez de Pablo AL, Gonzalez MC, Dieguez G, Gomez B, Lluch S. Reduction of cerebrovascular reactivity during hypercapnia. *Am J Physiol.* 1982; 242:R441–R446. [PubMed: 7081468]

- Lu H, Xu F, Grgac K, Liu P, Qin Q, VAN Zijl P. Calibration and validation of TRUST MRI for the estimation of cerebral blood oxygenation. *Magn Reson Med.* 2012; 67:42–49. [PubMed: 21590721]
- Maggio P, Salinet AS, Robinson TG, Panerai RB. Influence of CO₂ on neurovascular coupling: interaction with dynamic cerebral autoregulation and cere-brovascular reactivity. *Physiol Rep.* 2014; 2:e00280. [PubMed: 24760531]
- Mark CI, Slessarev M, Ito S, Han J, Fisher JA, Pike GB. Precise control of end-tidal carbon dioxide and oxygen improves BOLD and ASL cerebrovascular reactivity measures. *Magn Reson Med.* 2010; 64:749–756. [PubMed: 20648687]
- Murphy K, Birn RM, Handwerker DA, Jones TB, Bandettini PA. The impact of global signal regression on resting state correlations: are anti-correlated networks Introduced? *NeuroImage.* 2009; 44:893–905. [PubMed: 18976716]
- Nasrallah FA, Yeow LY, Biswal B, Chuang KH. Dependence of BOLD signal fluctuation on arterial blood CO₂ and O₂: implication for resting-state functional connectivity. *NeuroImage.* 2015; 117:29–39. [PubMed: 26003858]
- Nur E, Kim YS, Truijen J, VAN Beers EJ, Davis SC, Brandjes DP, et al. Cerebro-vascular reserve capacity is impaired in patients with sickle cell disease. *Blood.* 2009; 114:3473–3478. [PubMed: 19700663]
- Packard SD, Mandeville JB, Ichikawa T, Ikeda K, Terada K, Niloff S, et al. Functional response of tumor vasculature to PaCO₂: determination of total and microvascular blood volume by MRI. *Neoplasia.* 2003; 5:330–338. [PubMed: 14511404]
- Patterson, N. A robust, non-parametric method to identify outliers and improve final yield and quality. CS MANTECH; Boston: 2012.
- Peng T, Niazy R, Payne SJ, Wise RG. The effects of respiratory CO₂ fluctuations in the resting-state BOLD signal differ between eyes open and eyes closed. *Magn Reson Imaging.* 2013; 31:336–345. [PubMed: 22921940]
- Power JD, Barnes KA, Snyder AZ, Schlaggar BL, Petersen SE. Spurious but systematic correlations in functional connectivity MRI networks arise from subject motion. *NeuroImage.* 2012; 59:2142–2154. [PubMed: 22019881]
- Prisman E, Slessarev M, Han J, Poublanc J, Mardimae A, Crawley A, et al. Comparison of the effects of independently-controlled end-tidal PCO₂ and PO₂ on blood oxygen level-dependent (BOLD) fMRI. *J. Magn. Reson. Imaging.* 2008; 27:185–191.
- Puce A, Constable RT, Luby ML, McCarthy G, Nobre AC, Spencer DD, et al. Functional magnetic resonance imaging of sensory and motor cortex: comparison with electrophysiological localization. *J Neurosurg.* 1995; 83:262–270. [PubMed: 7616272]
- Rack-Gomer AL, Liu TT. Caffeine increases the temporal variability of resting-state BOLD connectivity in the motor cortex. *NeuroImage.* 2012; 59:2994–3002. [PubMed: 22032947]
- Segonne F, Dale AM, Busa E, Glessner M, Salat D, Hahn HK, et al. A hybrid approach to the skull stripping problem in MRI. *NeuroImage.* 2004; 22:1060–1075. [PubMed: 15219578]
- Segonne F, Pacheco J, Fischl B. Geometrically accurate topology-correction of cortical surfaces using nonseparating loops. *IEEE Trans Med Imaging.* 2007; 26:518–529. [PubMed: 17427739]
- Sicard K, Shen Q, Brevard ME, Sullivan R, Ferris CF, King JA, et al. Regional cerebral blood flow and BOLD responses in conscious and anesthetized rats under basal and hypercapnic conditions: implications for functional MRI studies. *J Cereb Blood Flow Metab.* 2003; 23:472–481. [PubMed: 12679724]
- Sled JG, Zijdenbos AP, Evans AC. A nonparametric method for automatic correction of intensity nonuniformity in MRI data. *IEEE Trans Med Imaging.* 1998; 17:87–97. [PubMed: 9617910]
- Slessarev M, Han J, Mardimae A, Prisman E, Preiss D, Volgyesi G, et al. Prospective targeting and control of end-tidal CO₂ and O₂ concentrations. *J Physiol.* 2007; 581:1207–1219. [PubMed: 17446225]
- Stefanovic B, Warnking JM, Rylander KM, Pike GB. The effect of global cerebral vasodilation on focal activation hemodynamics. *NeuroImage.* 2006; 30:726–734. [PubMed: 16337135]

- Tak S, Polimeni JR, Wang DJ, Yan L, Chen JJ. Associations of resting-state fMRI functional connectivity with flow-BOLD coupling and regional vasculature. *Brain Connect*. 2015; 5:137–146. [PubMed: 25384681]
- Tancredi FB, Hoge RD. Comparison of cerebral vascular reactivity measures obtained using breath-holding and CO₂ inhalation. *J Cereb Blood Flow Metab*. 2013; 33:1066–1074. [PubMed: 23571282]
- Tancredi FB, Gauthier CJ, Madjar C, Bolar DS, Fisher JA, Wang DJJ, et al. Comparison of pulsed and pseudocontinuous arterial spin-labeling for measuring CO₂-induced cerebrovascular reactivity. *J Magn Reson Imaging*. 2012; 36:312–321. [PubMed: 22544711]
- Thesen T, Leontiev O, Song T, Dehghani N, Hagler DJ JR, Huang M. Depression of cortical activity in humans by mild hypercapnia. *Hum Brain Mapp*. 2011; 33:715–726. [PubMed: 21500313]
- Tong Y, Frederick BD. Time lag dependent multimodal processing of concurrent fMRI and near-infrared spectroscopy (NIRS) data suggests a global circulatory origin for low-frequency oscillation signals in human brain. *NeuroImage*. 2010; 53:553–564. [PubMed: 20600975]
- Tong Y, Hocke LM, Fan X, Janes AC, de Frederick BB. Can apparent resting state connectivity arise from systemic fluctuations? *Front Hum Neurosci*. 2015; 9:285. [PubMed: 26029095]
- Tukey, JW. *Exploratory Data Analysis*. Addison-Wesley; 1977.
- Xu F, Uh J, Brier MR, Hart JJ, Yezhuvath US, Gu H, et al. The influence of carbon dioxide on brain activity and metabolism in conscious humans. *J Cereb Blood Flow Metab*. 2011; 31:58–67. [PubMed: 20842164]
- Yeo BT, Krienen FM, Sepulcre J, Sabuncu MR, Lashkari D, Hollinshead M, et al. The organization of the human cerebral cortex estimated by intrinsic functional connectivity. *J Neurophysiol*. 2011; 106:1125–1165. [PubMed: 21653723]
- Yuan H, Zotev V, Phillips R, Bodurka J. Correlated slow fluctuations in respiration, EEG, and BOLD fMRI. *NeuroImage*. 2013; 79:81–93. [PubMed: 23631982]
- Zappe AC, Uludag K, Oeltermann A, Ugurbil K, Logothetis NK. The influence of moderate hypercapnia on neural activity in the anesthetized nonhuman primate. *Cereb Cortex*. 2008; 18:2666–2673. [PubMed: 18326521]
- Ziyeh S, Rick J, Hetzel A, Mader I, Speck O. Blood oxygen level-dependent MRI of cerebral CO₂ reactivity in severe carotid stenosis and occlusion. *Stroke*. 2005; 36:751–756. [PubMed: 15705935]

Appendix A. Supplementary data

Supplementary data to this article can be found online at <http://dx.doi.org/10.1016/j.neuroimage.2016.02.051>.

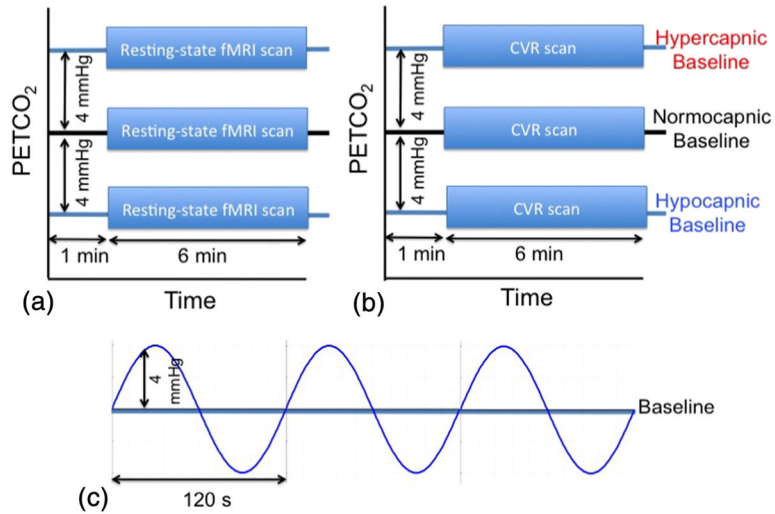


Fig. 1.

Experimental design. (a) Resting-state fMRI scans were carried out at three different basal capnic states, namely, hypercapnia, normocapnia (subject's natural baseline) and hypocapnia. The same capnic modulations were applied during measurements of cerebrovascular reactivity (CVR), seen in (b). During the CVR scans, a vasodilatory-vasoconstrictive vascular stimulus, in the form of sinusoidally modulated CO₂ (c), was administered over 6 min, spanning 3 periods of the sinusoid.

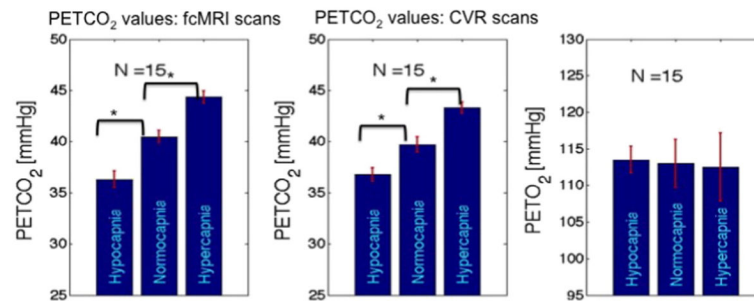


Fig. 2.

Basal PETCO₂ modulations and corresponding PETO₂ levels. In addition to the group-wise normocapnia level of 40 mm Hg CO₂, the desired basal PETCO₂ modulations of +4 mm Hg (hypercapnia) and -4 mm Hg (hypocapnia) were achieved, creating matched capnic conditions for the fcMRI and CVR runs. All capnic levels were significantly different from one another (asterisk indicates $p < 0.0001$), with error bars representing standard error. These modulations did not result in significant perturbations in PETO₂.

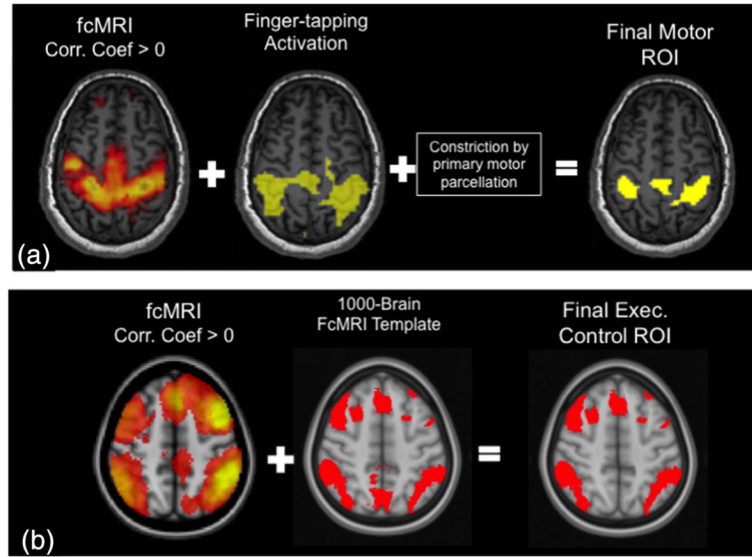


Fig. 3. Sample delineation procedure for region of interest (ROI) for a typical subject. The ROI used in the analyses is derived as follows: (a) motor ROI, defined as the intersection of (1) the motor network, (2) the finger-tapping functional scout and (3) the anatomical segmentation of Brodmann's Area 4; (b) control-network ROI, defined as the intersection between the thresholded fcMRI map and the control network template extracted from the 1000-brain fcMRI atlas. The left- and right control networks were first mapped separately based on left and right frontal and parietal seeds, with the seed region discarded from each intermediate connectivity map prior to the cross-hemisphere averaging to produce the final fcMRI map.

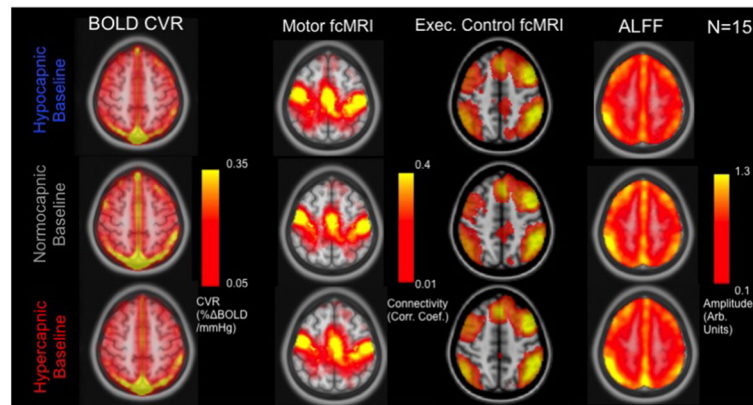


Fig. 4. Group-average CVR, functional connectivity and amplitude of low frequency fluctuation (ALFF) maps, at the tree basal vascular conditions, i.e. hypocapnia, normocapnia and hypercapnia. The hyperintensity in the posterior portion of the CVR maps is likely caused by venous contribution (superior sagittal sinus).

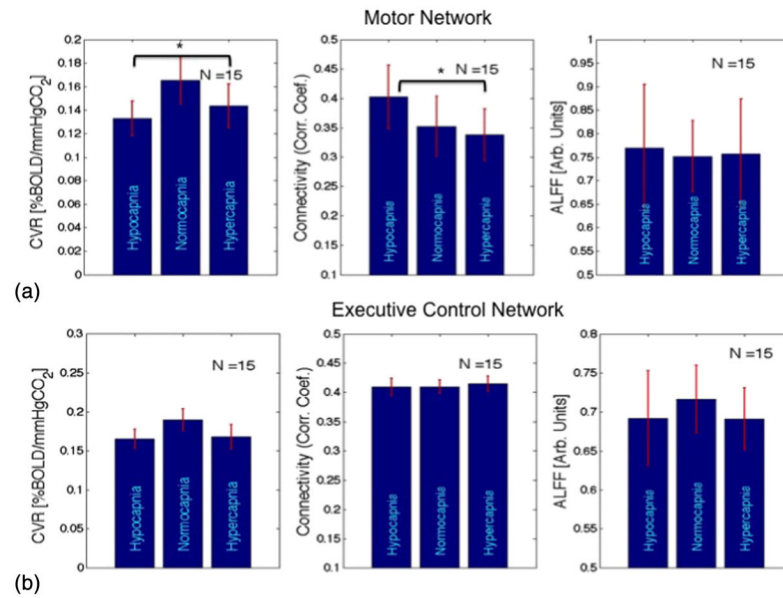


Fig. 5. Group-average CVR, functional connectivity and ALFF values across different capnic conditions. CVR was highest in normocapnia, reduced in the hypercapnic and hypocapnic baselines. However, in the motor network, functional connectivity consistently decreases with increasing PETCO₂. Asterisks mark differences with $p < 0.05$ based on a 3-level ANOVA.

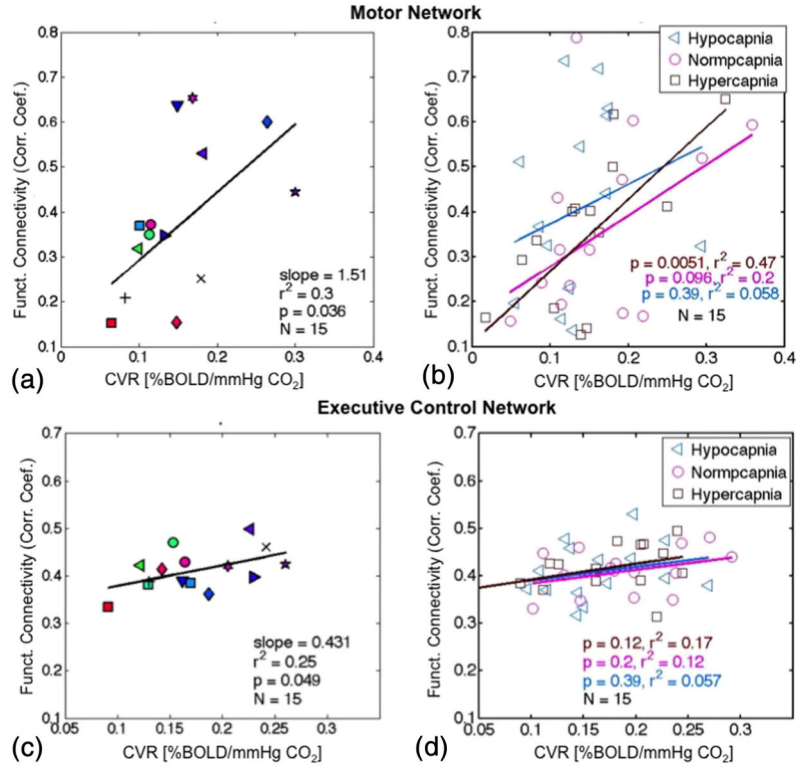


Fig. 6. The relationship between CVR and functional connectivity measurements. In (a) and (c), each filled symbol represents the value from one subject averaged across all vascular conditions. In (b) and (d), each symbol represents the value from one subject at each of the capnic conditions, which are color-coded identically in the symbols and lines.

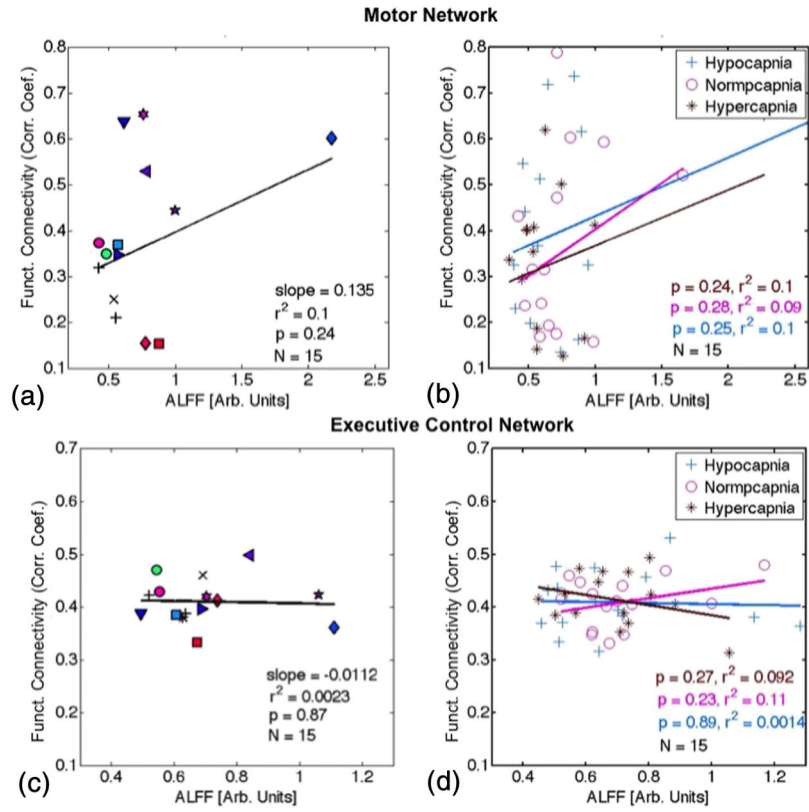
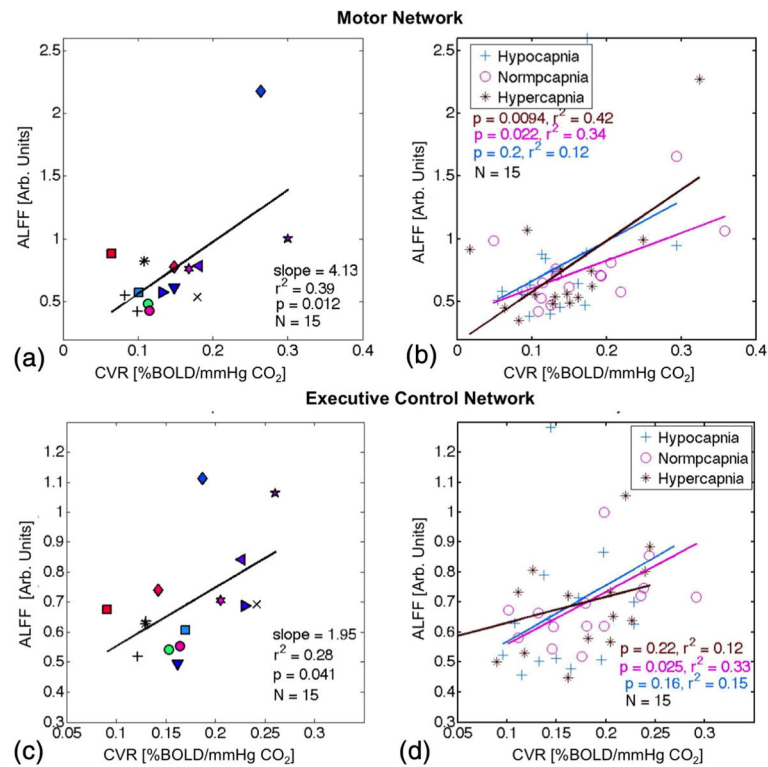


Fig. 7.

The relationship between connectivity and ALFF. In (a) and (c), each filled symbol represents the value from one subject averaged across all vascular conditions. In (b) and (d), each symbol represents the value from one subject at each of the capnic conditions, which are color-coded identically in the symbols and lines.

**Fig. 8.**

The relationship between ALFF and CVR. In (a) and (c), each filled symbol represents the value from one subject averaged across all vascular conditions. In (b) and (d), each symbol represents the value from one subject at each of the capnic conditions, which are color-coded identically in the symbols and lines.

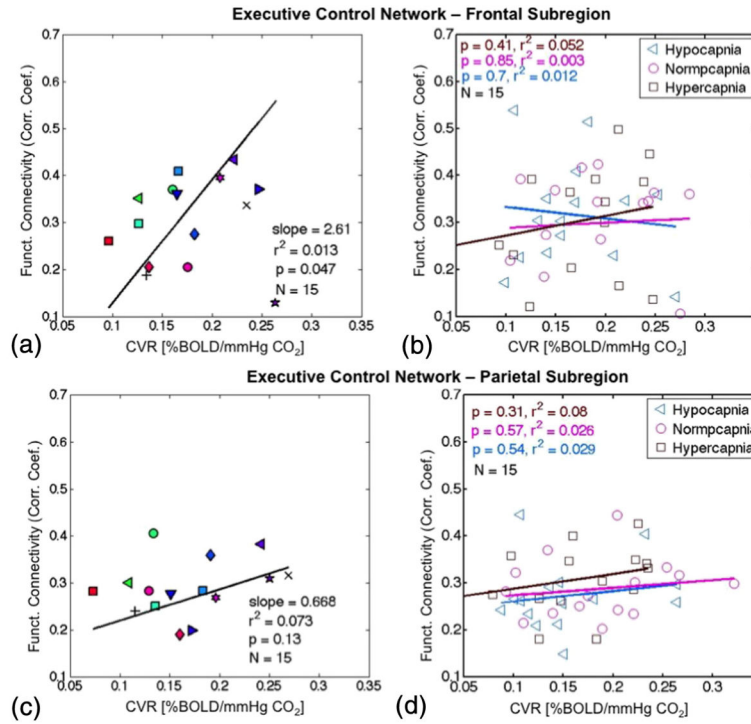


Fig. 9. Assessing fMRI–CVR associations for frontal and parietal nodes of the executive control network. In (a) and (c), each filled symbol represents the value from one subject averaged across all vascular conditions. In (b) and (d), each symbol represents the value from one subject at each of the capnic conditions, which are color-coded identically in the symbols and lines. The fMRI scores in the frontal component (a–b) of the control network exhibits significantly more pronounced CVR dependence than the parietal component (c–d).

Table 1

Physiological and motion measurements (mean and standard deviation) across various experimental conditions, averaged across the corresponding CVR and rs-fMRI scans. Heart and respiratory rates are computed from the scanner's physiological monitoring logs. Absolute motion is computed as the temporal mean of shifts between all frames and the reference frame, while relative motion is computed as mean shifts between frames.

	Hypocapnia	Normocapnia	Hypercapnia	Effect of capnic condition
Heart rate (Hz)	1.14 ± 0.20	1.10 ± 0.19	1.13 ± 0.18	<i>p</i> = 0.30
Respiration rate (Hz)	0.22 ± 0.07	0.25 ± 0.18	0.24 ± 0.09	<i>p</i> = 0.24
Motion (absolute, mm)	0.27 ± 0.19	0.23 ± 0.11	0.29 ± 0.04	<i>p</i> = 0.33
Motion (relative, mm)	0.05 ± 0.03	0.05 ± 0.02	0.06 ± 0.04	<i>p</i> = 0.23

Table 2

Seed selection procedure: motor and executive-control networks.

Network	Seed definition	Notes
Motor network	The overlap between: <ul style="list-style-type: none"> Finger-tapping task activation ROI Primary motor-cortex parcellation 	<ul style="list-style-type: none"> Seeds defined on a per-subject basis Connectivity to left and right seed computed separately Seed regions later excluded in mean connectivity estimation
Executive-control network	A 6-mm sphere located at <ul style="list-style-type: none"> The centroids of the superior-frontal and superior-parietal nodes defined by the 1000-brain atlas 	<ul style="list-style-type: none"> Seeds defined based on MNI152 atlas of executive-control network Left and right-control networks mapped separately first, then averaged across hemispheres Seed regions later excluded in mean connectivity estimation

Table 3

ANOVA results: capnia and subject dependence of CVR, functional connectivity and ALFF are assessed.

		CVR	Functional connectivity	ALFF
Motor network	Capnia	$p = \mathbf{0.05}$	$p = 0.23$	$p = 0.95$
	Subject	$p < \mathbf{0.0001}$	$p < \mathbf{0.0001}$	$p < \mathbf{0.0001}$
Executive control network	Capnia	$p = 0.11$	$p = 0.89$	$p = 0.66$
	Subject	$p < \mathbf{0.0001}$	$p = \mathbf{0.0007}$	$p < \mathbf{0.0001}$

Significant effects are marked in bold.